hydrology

MDPI

Article

Analyzing the December 2013 Metaponto Plain (Southern Italy) Flood Event by Integrating Optical Sensors Satellite Data

Teodosio Lacava [1,*], Emanuele Ciancia [2], Mariapia Faruolo [1], Nicola Pergola [1], Valeria Satriano [1] and Valerio Tramutoli [2]

[1] National Research Council, Institute of Methodologies for Environmental Analysis, C. da S. Loja, 85050 Tito Scalo (PZ), Italy; mariapia.faruolo@imaa.cnr.it (M.F.); nicola.pergola@imaa.cnr.it (N.P.); valeria.satriano@imaa.cnr.it (V.S.)

[2] School of Engineering, University of Basilicata, Via dell'Ateneo Lucano, 10, 85100 Potenza, Italy; emanuele.ciancia@imaa.cnr.it (E.C.); valerio.tramutoli@unibas.it (V.T.)

* Correspondence: teodosio.lacava@imaa.cnr.it; Tel.: +39-0971-427242

Received: 5 July 2018; Accepted: 5 August 2018; Published: 7 August 2018

Abstract: Timely and continuous information about flood dynamics are fundamental to ensure an effective implementation of the relief and rescue operations. Satellite data provided by optical sensors onboard meteorological satellites could have great potential in this framework, offering an adequate trade-off between spatial and temporal resolution. The latest would benefit from the integration of observations coming from different satellite systems, also helping to increase the probability of finding cloud free images over the investigated region. The Robust Satellite Techniques for detecting flooded areas (RST-FLOOD) is a sensor-independent multi-temporal approach aimed at detecting flooded areas which has already been applied with good results on different polar orbiting optical sensors. In this work, it has been implemented on both the 250 m Moderate Resolution Imaging Spectroradiometer (MODIS) and the 375 m Suomi National Polar-orbiting Partnership (SNPP) Visible Infrared Imaging Radiometer Suite (VIIRS). The flooding event affecting the Basilicata and Puglia regions (southern Italy) in December 2013 has been selected as a test case. The achieved results confirm the RST-FLOOD potential in reliably detecting, in case of small basins, flooded areas regardless of the sensor used. Flooded areas have indeed been detected with similar performance by the two sensors, allowing for their continuous and near-real time monitoring.

Keywords: flood; remote sensing; data integration; RST-FLOOD; MODIS; VIIRS; optical data

1. Introduction

Among natural disasters, floods are more easily investigable using satellite data. In 2016, among the 36 activations of the International Charter "Space & Major Disasters", 17 (i.e., 44%) of them were related to floods [1], demonstrating the effectiveness of the information that satellite remote sensing can provide in this context. Several indications can be furnished in all the phases (i.e., mitigation, preparedness, response, recovery) of the flood risk management cycle. In particular, among the different possible contributions, information about flood mapping and monitoring activities can be useful for all the above-mentioned phases [2–4]. A flood map is prepared during/after a flood occurrence in order to delineate the inundated areas, while flood maps of different times are suitable for monitoring water expansion and regression [2,3]. Moreover, multi-temporal maps can aid in detecting critical spatial changes in flood hazards and vulnerability over time. These products can be used for flood prone area delineation in order to prevent future floods, providing crucial information to identify appropriate protection measures and strategies for risk mitigation and producing efficient

response plans [5]. Once a flood event occurs, emergency planners and rescuers can use inundation maps to detect the most affected areas, then identify evacuation routes and plan the assistance and aid. During the recovery stage, flood maps can support the identification of places for reconstruction and multi-date maps aid in the monitoring of community rebuilding [6].

Microwave and optical-band data have been widely used to produce flooding maps, exploiting the specific advantages of each spectral band and technology used [7,8]. Microwave sensors enable an all-day (i.e., 24 h) and all-weather detection capability, with spatial resolution ranging from few meters to dozens of kilometers when moving from active to passive technologies, respectively [5]. On the other hand, active sensors (e.g., Synthetic Aperture Radar (SAR)) allow for medium-long temporal frequency (up to five to six days), while passive radiometers have sub-daily temporal resolution [5]. Therefore, SAR data can provide infrequent detailed information about small-scale flooded areas, while passive microwave data could represent the most suitable solution if timely information is required for investigating large-scale flooding events [9]. Optical sensors onboard polar satellites, usually deployed in satellite constellation, can assure the better trade-off among spectral/spatial/temporal resolutions useful for a near real-time and continuous monitoring of flooded areas [10,11]. Obviously, cloud cover can fully hamper any kind of acquisition in this spectral region, limiting the applicability of this data. Hence, the integration of data acquired by sensors operating at different wavelengths is preferred to avoid such an issue, as well as to make the most of their potential [12].

The Robust Satellite Techniques (RST) [13] is a general multi-temporal satellite data analysis methodology that has already been applied for detecting flooded areas (RST-FLOOD [12,14]) on Advanced Very High Resolution Radiometer (AVHRR) and Moderate Resolution Imaging Spectroradiometer (MODIS) data. Both of these sensors acquire data in the Visible (VIS) and Near Infrared (NIR) regions, allowing for flooded area detection thanks to the particular spectral behavior of water at these wavelengths. Compared to other common land cover and features (like bare or vegetated soils), water generally shows a reflectance (R) in the NIR lower than in the VIS region, with the latter that corresponds for both sensors to the Red (RED) portion of the electromagnetic spectrum. Therefore, in the presence of water bodies or flooded areas, values lower than the surroundings have to be expected for the combinations of spectral reflectances acquired in the VNIR (VIS and NIR) region, like the ratio R_{NIR}/R_{VIS} [15,16] or the difference R_{NIR}-R_{VIS} [17].

In this paper, we further assess the RST-FLOOD performance in detecting flooded areas by investigating a few days of the flood event that affected the Basilicata and Puglia regions (southern Italy—Figure 1) in December 2013 [18–23]. In order to investigate this event, we firstly implemented the MODIS-based approach using data acquired in its first two channels at 250 m of spatial resolution. In the previous work [12], the feasibility of this data providing reliable information about flooded areas was only preliminarily explored, referring to a much larger event than the one analyzed here in terms of flood extent. Then, exploiting the RST-FLOOD inherent characteristics, we exported the proposed approach on Suomi National Polar-orbiting Partnership (SNPP) Visible Infrared Imaging Radiometer Suite (VIIRS) imagery. The VIIRS instrument extends and improves upon a series of measurements initiated by its operational and research predecessors, the AVHRR flown on board multiple National Oceanic and Atmospheric Administration (NOAA) and Meteorological Operational (Metop) satellites, and the National Aeronautics and Space Administration (NASA) MODIS, aboard the Terra and Aqua satellites, due to its better spatial and spectral resolution as well as radiometric accuracy and stability. The accuracy of the achieved results has been evaluated through a comparison analysis with a Landsat Enhanced Thematic Mapper Plus image (ETM+ on Landsat 7) acquired concurrently with MODIS and VIIRS data.

The main aim of this study is to assess the potential of RST-FLOOD, when implemented on medium spatial resolution images, in effectively analyzing floods occurring within small catchments.

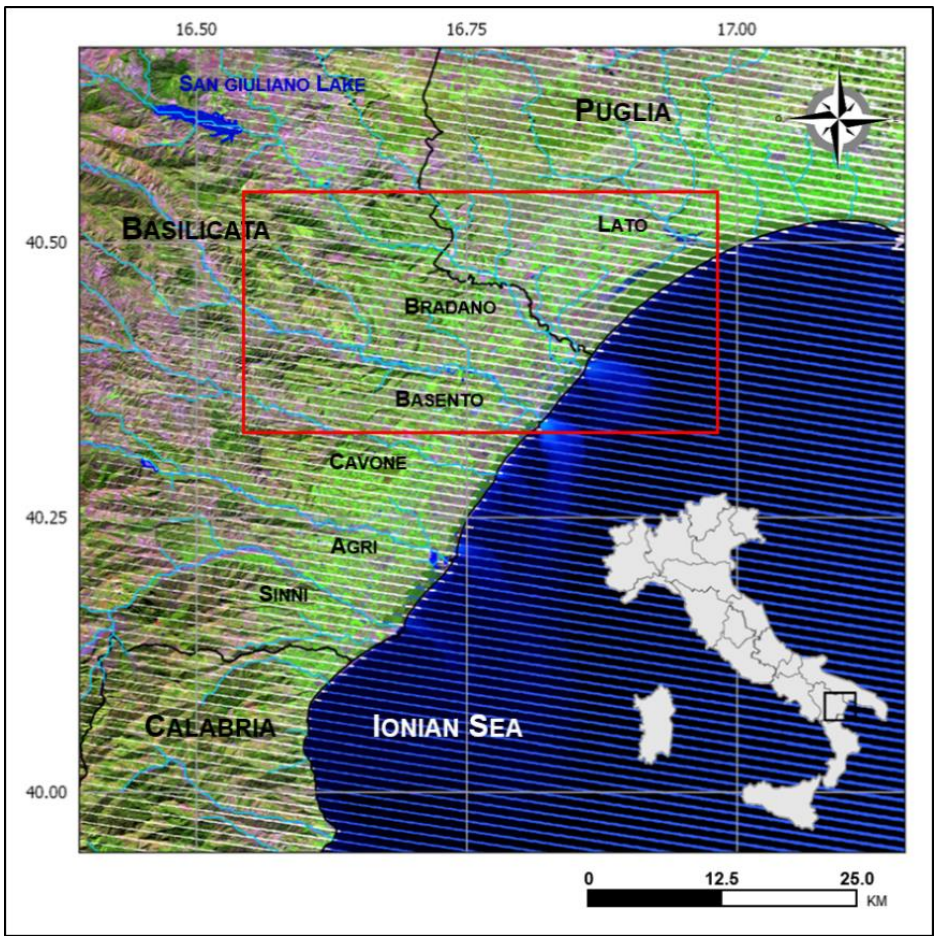

Figure 1. Localization of the Region of Interest (ROI). In the background, the Landsat Enhanced Thematic Mapper Plus (Landsat 7 ETM+) false-color (R = Short Wave InfraRed-SWIR; G = NIR; B = RED) composite image of 5 December 2013 at 9:31 GMT. The red box is the area used in the text.

2. Study Area

A flood event affected a large portion of the Metaponto plain, in the southeastern part of the Basilicata region (southern Italy), including a subset of the Puglia region (Figure 1), in the first week of December 2013 [18,19,23]. This event was caused by a significant amount of rainfall due to the "Ciclone Nettuno" storm that occurred in the Basilicata region between 30 November and 3 December 2013 [24]. A medium cumulative precipitation value of 150 mm was registered for the whole Basilicata Region between 1 and 2 December 2013, with peaks above 200 mm in the Metaponto plain [18,21]. The Sinni, Agri, Cavone, Basento and Bradano rivers in Basilicata and the Lato River in Puglia flooded in several points along their path, as well as in correspondence of the freeway "Strada Statale 106", causing its closure and serious damage to farms and agricultural crops [18]. All the rivers involved in the event are strongly seasonally dependent, with maximum hydrometric levels usually reached between the late fall and the early spring, and minimum levels reached in summer at cross-sections lower than 100 m [25]. Therefore, the studied event represents a suitable test case for evaluating the potential of medium-resolution optical sensors in investigating small-scale floods.

3. Data and Methods

3.1. Satellite Data

MODIS data acquired in the first two bands (i.e., channel 1, VIS, at 0.62–0.67 μm and channel 2, NIR, at 0.841–0.876 μm) at 250 m of spatial resolution were used in this work. In more detail, imagery acquired by the sensor onboard the Aqua satellite in the 12:00–14:00 GMT temporal range, for the month of December in the 2002–2016 period have been investigated. MODIS Level 1B (MYD02QKM)

and geolocation (MYD03) data directly produced at the satellite receiving station of the Institute of Methodologies for Environmental Analysis (IMAA), located in Tito Scalo (Basilicata region, southern Italy), have been processed. These data have been produced by running the Community Satellite Processing Package (CSPP) software with antenna data directly acquired. Level 1B and geolocation data downloaded from the Level-1 and Atmosphere Archive & Distribution System (LAADS) Distributed Active Archive Center (DAAC) archive [26] have been also used to fill any gaps in the analyzed historical series.

Similarly, for VIIRS, data collected in the first two imagery bands (i.e., I1, VIS, at 0.60–0.68 μm and I2, NIR, at 0.85–0.88 μm) and the thermal infrared (TIR) imagery one (I5, TIR, at 10.5–12.4 μm) at 375 m of spatial resolution were investigated. In particular, acquisitions coming from the SNPP satellite in the same daily temporal range of Aqua were considered for the month of December in the 2012–2016 period. Also for VIIRS, the SNPP Sensor Data Record (SDR) and the I-band terrain-corrected geolocation (GITCO) data directly produced at the Institute of Methodologies for Environmental Analysis (IMAA) receiving station, which was downloaded from the NOAA Comprehensive Large Array-data Stewardship System (CLASS) archive [27], have been exploited to populate the historical series.

Finally, in absence of in situ ground truth data, the Landsat 7 ETM+ image acquired on 5 December 2013 at 9:31 GMT over the ROI and downloaded from the U.S. Geological Survey (USGS) portal [28] (Figure 1), was used to assess the accuracy of the achieved results. The RGB false color (R = SWIR, 1.55–1.75 μm; G = NIR, 0.775–0.90 μm; B = RED, 0.63–0.69 μm) of such an image, related to the ROI, is shown in Figure 1. In order to better highlight the area most affected by the water presence, the Normalized Difference Vegetation Index (NDVI) has been computed, looking for values below zero, which should correspond to water affected areas [29], including both flooded pixels and permanent water. A Boolean (water/no water) mask was produced and shown in Figure 2.

An area of about 105 km^2 has been recognized as affected by water presence, including permanent waters related both to rivers and the San Giuliano Lake included within the ROI.

Figure 2. In green, the pixels of the Landsat 7 ETM+ image, shown in Figure 1, recognized as water affected are depicted (see text).

3.2. RST-FLOOD

The RST-FLOOD approach has already been implemented on AVHRR and MODIS data exploiting the above cited particular spectral behaviour of water in the VNIR (VIS and NIR) region of the electromagnetic spectrum [12,14]. This has led to the development of the two following Absolutely Local Index of Change of the Environment (ALICE—[13]) indices:

$$\mathrm{ALICE}_{\mathrm{NIR-VIS}}(x,y,t) = \frac{R_{\mathrm{NIR-VIS}}(x,y,t) - \mu_{\mathrm{NIR-VIS}}(x,y)}{\sigma_{\mathrm{NIR-VIS}}(x,y)}, \quad (1)$$

$$\mathrm{ALICE}_{\mathrm{NIR/VIS}}(x,y,t) = \frac{R_{\mathrm{NIR/VIS}}(x,y,t) - \mu_{\mathrm{NIR/VIS}}(x,y)}{\sigma_{\mathrm{NIR/VIS}}(x,y)}, \quad (2)$$

where $R_{\mathrm{NIR-VIS}}(x,y,t)$ (or $R_{\mathrm{NIR/VIS}}(x,y,t)$) is the reflectance difference (ratio) signal measured at time t for each pixel (x,y) of the analyzed satellite scene, $\mu_{\mathrm{NIR-VIS}}(x,y)$ (or $\mu_{\mathrm{NIR/VIS}}(x,y)$) and $\sigma_{\mathrm{NIR-VIS}}(x,y)$ (or $\sigma_{\mathrm{NIR/VIS}}(x,y)$), the named reference fields, are, respectively, the "normal" value expected for the signal and its natural variability. They are both computed by processing a multi-year dataset of co-located cloud-free imagery, collected under homogeneous observational conditions (e.g., around the same time of day and during the same month of the year). For its inherent formulation, each ALICE provides, at the pixel level, a measure of the deviation of the recorded signal from its expected (in unperturbed or normal conditions) value and automatically compares this deviation with its normal variability, which includes all the possible noise sources not related to the event being monitored. For example, the normal signal variability (i.e., the standard deviation reference field) is high for those pixels characterized both by the presence of water and land, because they are likely to be affected by a high signal fluctuation due to both residual geo-location errors and the natural cross-section changes. Therefore, for those areas, anomalous ALICE values will only be detected when high signal deviation from the expected one will be measured. In any case, in correspondence to flooded areas, negative $\mathrm{ALICE}_{\mathrm{NIR-VIS}}(x,y,t)$ (and $\mathrm{ALICE}_{\mathrm{NIR/VIS}}(x,y,t)$) values should be observed.

Moreover, for their construction, both ALICE indices are standardized variables that, as the number (N) of the records increases, tend toward a Gaussian like distribution. Under this hypothesis, values of $\mathrm{ALICE}_{\mathrm{NIR/VIS}}$ (or $\mathrm{ALICE}_{\mathrm{NIR-VIS}}$) <-2 can be associated to rare events (probability of occurrence less than 2.5%) and values <-3 to very rare events (probability of occurrence less than 0.13%). Hence, statistically significant signal anomalies are expected for $\mathrm{ALICE}_{\mathrm{NIR/VIS}}$ (or $\mathrm{ALICE}_{\mathrm{NIR-VIS}}$) <-2 at least, with an increasing level of confidence when moving to the lowest ones (i.e., −3, −4) [12,14,24].

In order to investigate the selected flood event, the above-cited MODIS and VIIRS historical temporal series were separately processed, firstly generating their corresponding reference fields (i.e., temporal mean and standard deviation) for both difference and ratio signals, and then looking for signal anomalies in the event images.

During the generation of the reference fields and during the change detection step, cloudy pixels were identified and discarded from the detection step by implementing the One Channel Algorithm (OCA) method [30,31]. Such an approach, still based on the RST prescriptions, analyzes the historical series of MODIS channel 2 to identify clouds as statistically high reflectivity objects, or VIIRS I5 data to identify them as statistically cold bodies. With regards to cloud shadows, after a visual inspection of images within the used dataset, a simple 2 km (i.e., five-and six-pixel for MODIS and VIIRS, respectively) buffer around the detected clouds has been applied, thus ensuring a good trade-off between the possibility to produce false positives and omission errors.

4. Results

Two almost concurrently acquired imagery for the first two cloud-free days over the ROI by MODIS and VIIRS have been analyzed in terms of ALICE indices computation (Equations (1) and (2)). In detail, the results investigating the MODIS imagery of 4 December 2013 at 12:25 GMT and 5 December at 11:30 GMT are presented and discussed in Section 4.1, while those referring to the VIIRS sensor, 4 December at 12:10 GMT and 5 December at 11:50, are shown in Section 4.2. Finally, Section

4.3 is focused on the comparison analysis among results achieved in the previous two sections with the Landsat 7 ETM+ image shown in Figure 1.

4.1. MODIS RST-FLOOD

The RST-FLOOD maps produced by analyzing the two above-mentioned MODIS data are shown in Figure 3, where in the top panels (Figure 3a,b), the areas flagged as anomalous using the $ALICE_{NIR\text{-}VIS}$ index (i.e., Equation (1)) are shown, while those related to the ratio index (i.e., Equation (2)) are plotted in Figure 3c,d. In all the maps, indices values less than −2 are depicted in violet and orange colors when the difference and ratio indices have been applied, respectively.

Several anomalous pixels have been detected by the RST-FLOOD indicators in all the output maps. These pixels are mostly located along the Basento and Lato rivers and are in good agreement with the local information about the flood localization [18,21,22,32], thus indicating that it can be associated to the inundated zones. Moreover, a difference between the two indicators can be observed, with a higher sensitivity of the $ALICE_{NIR\text{-}VIS}$ to the flood inundated area (see areas along the Basento and Lato rivers), as well as to the effect of turbid waters in the San Giuliano lake (see Table 1). Concerning flood dynamics, a lesser number of anomalous pixels has been identified in the maps of 5 December 2013 by both indices (Table 1). In more detail, an area of about 16 km² was detected as flooded on 4 December 2013, decreasing to 12 km² the next day.

In order to provide a deeper view of the achieved results, a magnification of the area within the red box of Figure 1 is plotted in Figure 4, where for each of the analyzed MODIS images, the results achieved by combining both the indices are highlighted. This aggregation allowed for the better definition of the potentially flooded areas, while the common detections (namely the pixels flagged as anomalous by both indices—green pixels in Figure 4), may be associated to the definitely flooded areas. Furthermore, in these maps, the temporal persistence of the anomalous area is evident, as well as the better sensitivity of the $ALICE_{NIR\text{-}VIS}$ index than the $ALICE_{NIR/VIS}$ one.

Table 1. Number of anomalous pixels identified by the two ALICE indices in the two analyzed MODIS imagery.

	$ALICE_{NIR\text{-}VIS}$	$ALICE_{NIR/VIS}$
4 December 2013	219	98
5 December 2013	185	58

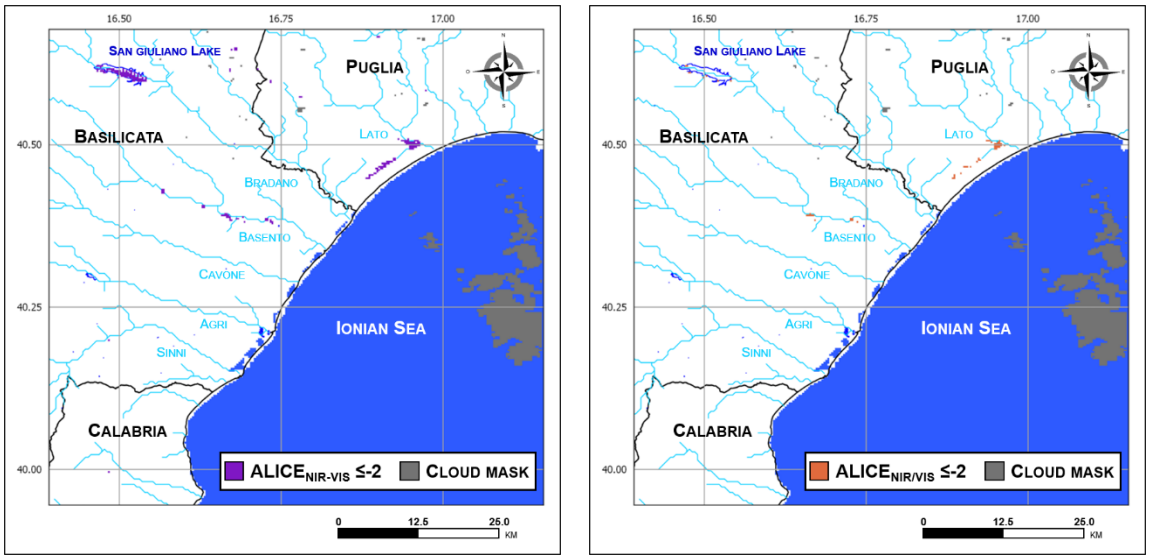

(**a**) (**b**)

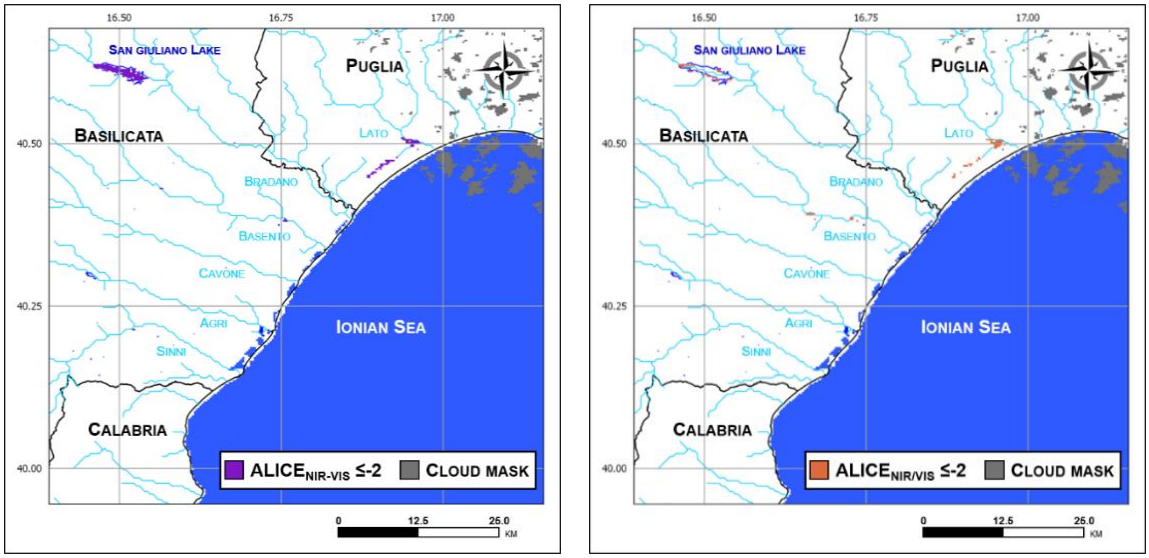

(**c**) (**d**)

Figure 3. Anomalous pixels detected by Moderate Resolution Imaging Spectroradiometer (MODIS)-based Robust Satellite Techniques for detecting flooded areas (RST-FLOOD) using: (**a**) Absolutely Local Index of Change of the Environment Near Infrared-Visible ($ALICE_{NIR-VIS}$), (**b**) $ALICE_{NIR/VIS}$ on 4 December 2013 at 12:25 GMT and (**c**) $ALICE_{NIR-VIS}$, (**d**) $ALICE_{NIR/VIS}$ on 5 December 2013 at 11:30 GMT.

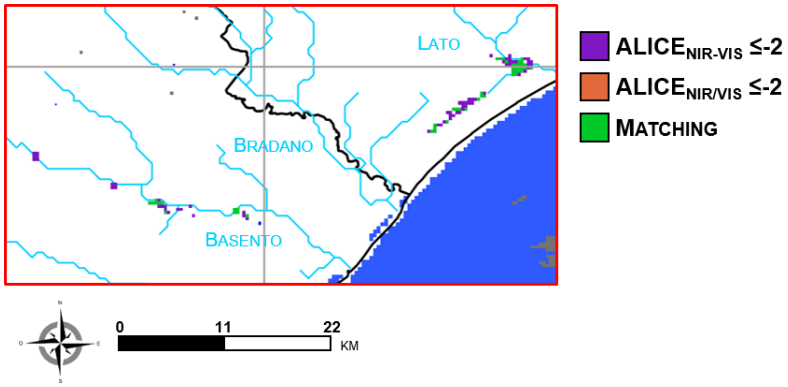

(**a**)

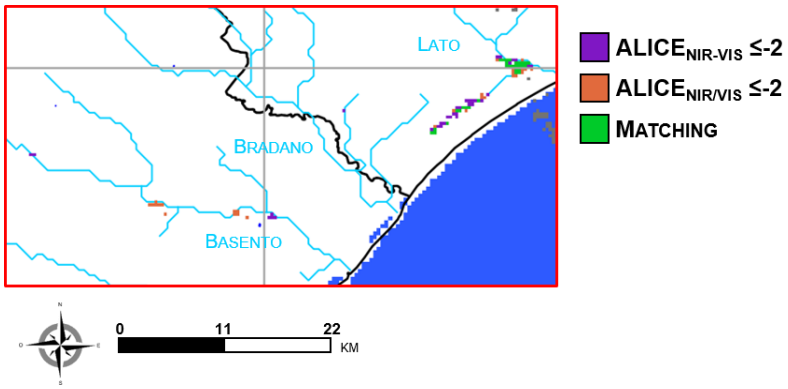

(**b**)

Figure 4. Anomalous pixels detected within the red box shown in Figure 1 by MODIS-based RST-FLOOD on (**a**) 4 December 2013 at 12:25 GMT and (**b**) 5 December 2013 at 11:30 GMT using $ALICE_{NIR-VIS}$ (violet pixels) and $ALICE_{NIR/VIS}$ (orange pixels). In green, the pixels detected as anomalous by both indices are highlighted.

4.2. VIIRS RST-FLOOD

Figure 5 shows the anomalous pixels identified within the ROI by implementing RST-FLOOD on VIIRS data. First, it is interesting to note that, when compared to MODIS, the two RST-FLOOD indices seem to show a higher sensitivity to flooding and to not significantly differ in terms of detected anomalies, as revealed by the analysis of the numbers reported in Table 2. In detail, an averaged area of approximately 52 km^2 was detected as flooded, almost three times higher than the one previously identified using MODIS. Although the VIIRS VNIR bands had lower spatial resolution than the MODIS one, the implementation of RST-FLOOD on VIIRS allowed for the detection of a larger number of anomalous pixels, not only along the Basento and Lato rivers, but also close to Cavone, Agri and Sinni, most likely due to the flooding. The almost equivalent number of detected pixels in two days confirm this high sensitivity, indicating that the effect of the flood was still detectable on 5 December. Concerning the San Giuliano Lake, the effect of suspended sediments is still present, even with a reduced impact. Finally, some spurious effects are also observable in the correspondence of a few pixels not close to riverbeds, disappearing when higher confidence levels of RST-FLOOD indices are used.

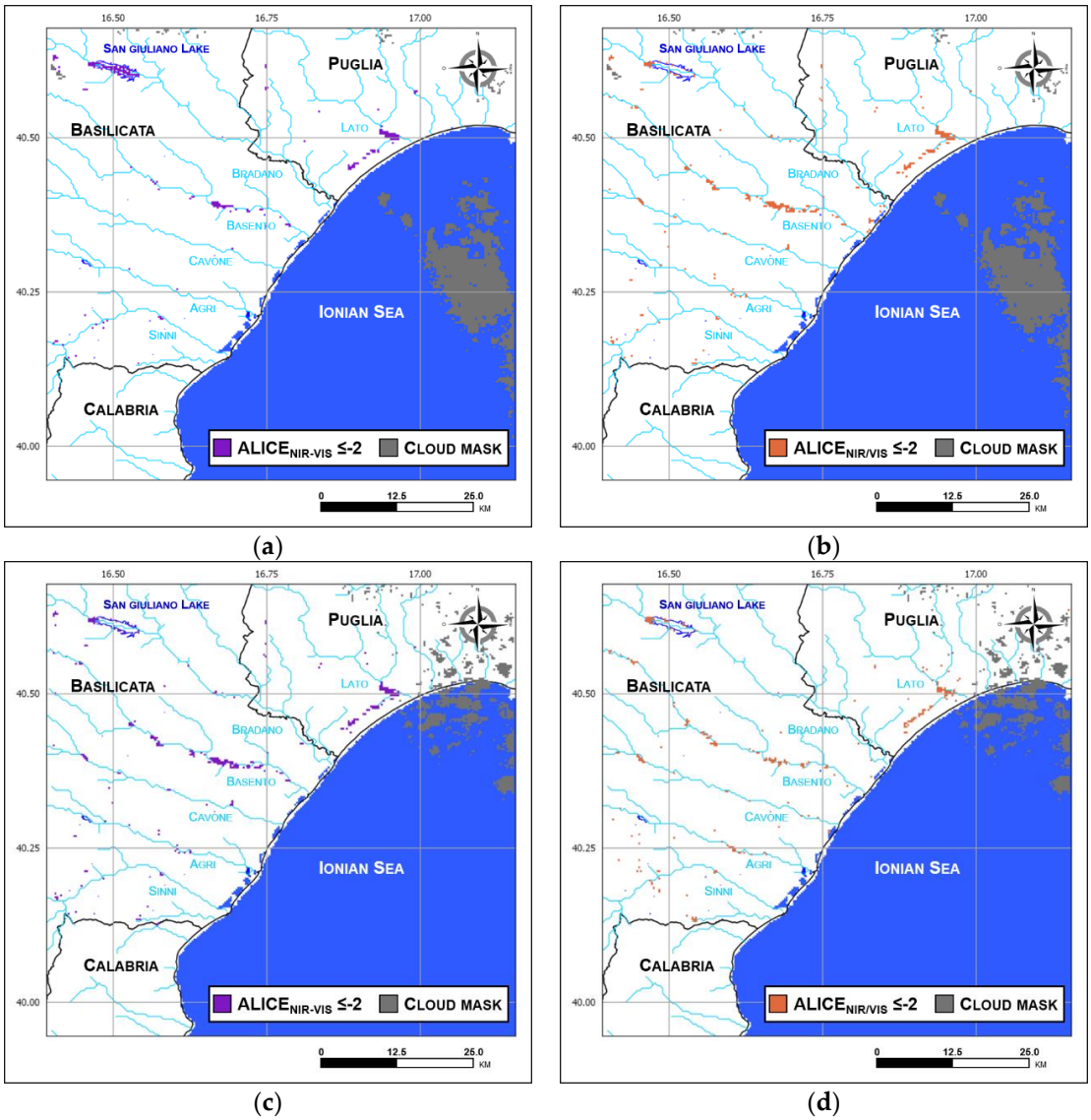

Figure 5. Anomalous pixels detected by Visible Infrared Imaging Radiometer Suite (VIIRS)-based RST-FLOOD using: (**a**) ALICE$_{NIR-VIS}$, (**b**) ALICE$_{NIR/VIS}$ on 4 December 2013 at 12:10 GMT and (**c**) ALICE$_{NIR-VIS}$, (**d**) ALICE$_{NIR/VIS}$ on 5 December 2013 at 11:50 GMT.

Table 2. Number of anomalous pixels identified by the two ALICE indices in the two analyzed VIIRS imagery.

	$ALICE_{NIR-VIS}$	$ALICE_{NIR/VIS}$
4 December 2013	214	272
5 December 2013	262	243

The magnification of the areas mainly affected by the event as detected by VIIRS have been taken into account and reported in Figure 6. The maps shown in this figure provide a clear confirmation of the considerations discussed above for MODIS, emphasizing the advantage in coupling the detections provided by the two RST-FLOOD indices, both in detecting the definitely flooding affected areas (green pixels in Figure 6) and improving the delimitation of their extent.

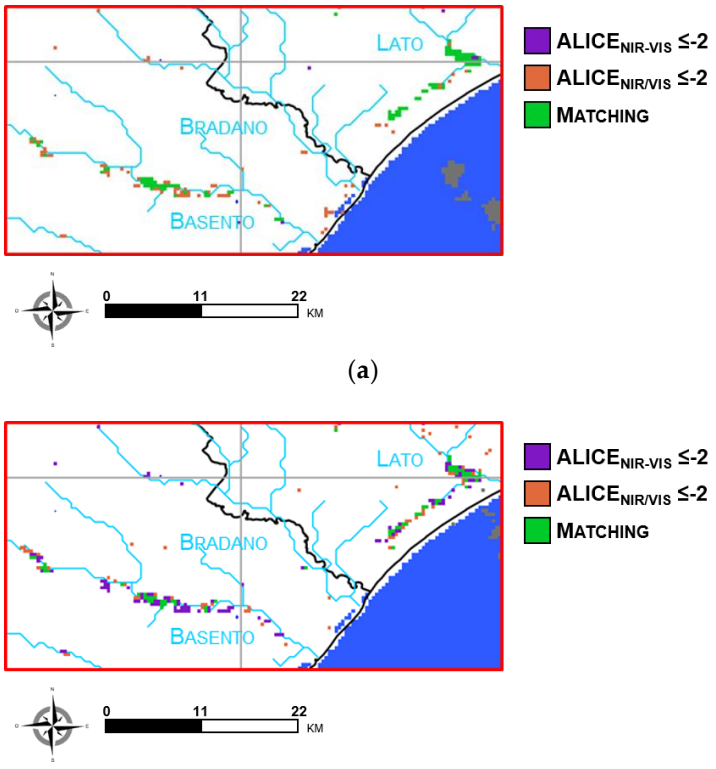

Figure 6. Anomalous pixels detected within the red box shown in Figure 1 by VIIRS-based RST-FLOOD on (**a**) 4 December 2013 at 12:10 GMT and (**b**) 5 December 2013 at 11:52 GMT using $ALICE_{NIR-VIS}$ (violet pixels) and $ALICE_{NIR/VIS}$ (orange pixels). In green, the pixels detected as anomalous by both indices are highlighted.

4.3. Comparison with Landsat

To assess the reliability of the proposed approach, the Landsat 7 ETM+ image of 5 December 2013, at 9:31 GMT, was exploited (Figure 1). In Figure 7a, a magnification of the area within the red box in Figure 1 is plotted, using the Boolean mask already plotted in Figure 2 in the background, where water affected areas are clearly visible along the Basento and Lato rivers, notwithstanding no data acquisition due to the Landsat 7's Scan Line Corrector (SLC) failure. An area of about 28 km^2 was identified as water affected within the investigated box (green pixels in Figure 7a).

The RST-FLOOD results carried out for 5 December 2013 have been superimposed on those areas aggregating MODIS and VIIRS detections (at 11:30 GMT and 11:52 GMT, respectively) achieved with the same ALICE index (Figure 7b,c), estimating an area ranging between 15 and 18 km^2 when the ratio (Figure 7c) and the difference (Figure 7b) index is used, respectively. Considering all the Landsat 7 water affected pixels depicted in Figure 7a as a benchmark for assessing the extension of flooded

areas, a maximum underestimation of about 46% was computed for RST-FLOOD. The large difference in terms of spatial resolution among ETM+ and the two optical sensors used in this work forms the basis of this result [12]. Spurious and isolated ETM+ water affected pixels cannot be detected at the spatial resolution allowed by MODIS and VIIRS. Moreover, even when those pixels are aggregated, their total contribution in terms of sub-pixel effect can provide a result lower than the expected value as defined by RST-FLOOD, and therefore they are not identified as anomalous. On the other hand, such an outcome is quite relevant, because it confirms the potential of the proposed approach in effectively detecting the presence of flooded areas notwithstanding the medium spatial resolution of the used data. Furthermore, concerning Landsat 7 water affected pixels, it is worth mentioning that they also take into account permanent water, as well as other effects not directly ascribable to water presence.

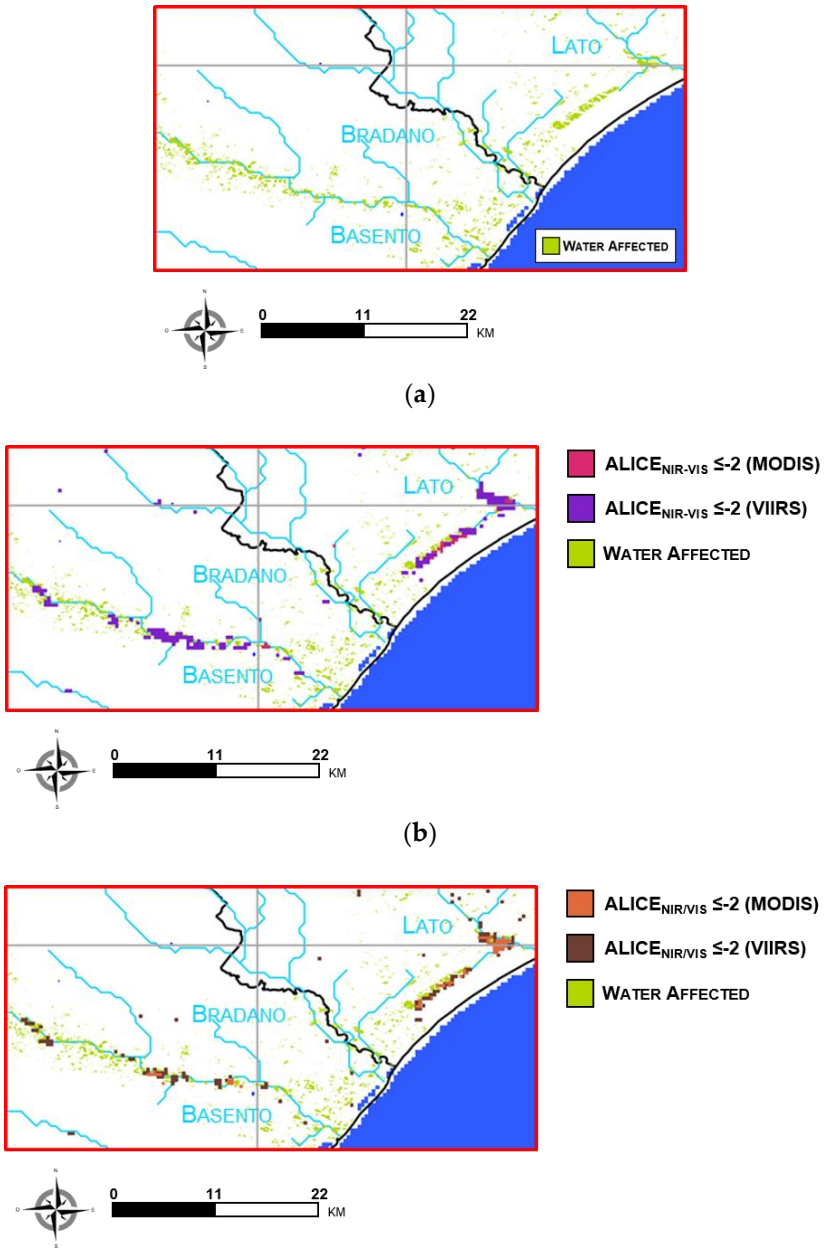

Figure 7. (**a**) Subset of the image shown in Figure 2 highlighting water affected pixels; (**b**) anomalous pixels detected by ALICE$_{NIR-VIS}$ on 5 December 2013 at 11:30 GMT for MODIS (pink) and at 11:52 GMT for VIIRS (violet); (**c**) anomalous pixels detected by ALICE$_{NIR/VIS}$ on 5 December 2013 at 11:30 GMT for MODIS (orange) and at 11:50 GMT for VIIRS (brown).

In any case, such a comparison shows the satisfactory capability of the proposed approach in detecting flooded areas regardless of the sensors used, and the different sensitivities of RST-FLOOD indicators when implemented on MODIS and VIIRS imagery. These aspects assume great relevance in detecting flooded areas by optical satellite data, reinforcing the great usefulness of implementing an integrated satellite system within the flood hazard management cycle, allowing for a more detailed identification of flooded areas and a continuous monitoring of the ongoing phenomenon on a large spatial scale. Advantages arising from such an integration are clearly observable when analyzing Figure 8, where the outputs produced by applying the same index on both of the sensors for the two available images are shown. An area of about 80 km^2 has been recognized as flooded in the two days examined by both MODIS and VIIRS sensors through the ALICE$_{\text{NIR-VIS}}$ index implementation, while 72 km^2 has been detected by the ALICE$_{\text{NIR/VIS}}$ index, with the main difference due to the pixel issues related to the San Giuliano turbid waters.

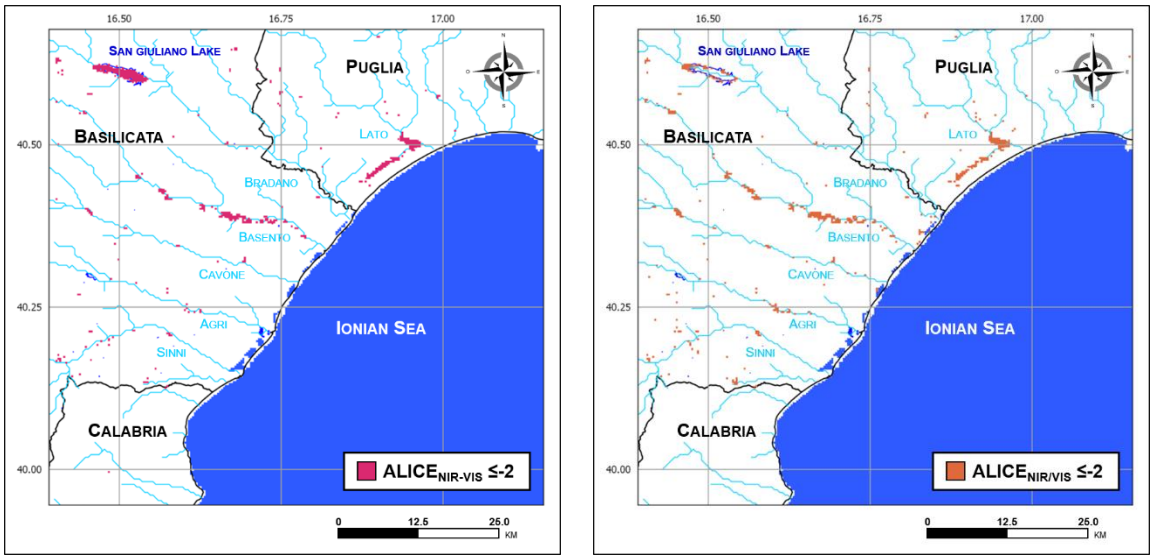

Figure 8. (**a**) Flooded areas detected within the Region of Interest (ROI) by integrating results achieved by ALICE$_{\text{NIR-VIS}}$ implemented on MODIS and VIIRS data for the two investigated days; (**b**) as in (**a**) using the ALICE$_{\text{NIR/VIS}}$.

5. Discussion

Timely and continuous information about flood dynamics is fundamental to ensure an effective implementation of relief and rescue operations. Using data acquired by optical sensors onboard meteorological satellites for flood detection and monitoring may be detrimental due to cloud cover that can hamper any kind of acquisition. Despite this limitation, there are several advantages that make optical data a good complement to other satellite-based systems, such as: (i) the large swath that allows for both large area coverage and high temporal resolution; (ii) a medium spatial resolution (in the order of hundreds of meters) useful for detecting medium-major flood events; and (iii) the deployment in satellites constellation that further enables an increase in revisiting time. In addition, sensors operating in different spectral regions that can complement the information acquired using optical data are often present aboard meteorological satellites [33]. Both MODIS and VIIRS, the optical sensors considered in this work, show almost all of the above-cited features, making them suitable for flooded area detection. While the MODIS capability in this framework has been largely demonstrated [11], there are only a few works based on VIIRS I-band data [9,34,35].

In this work, we implemented the RST-FLOOD approach on MODIS and VIIRS daytime data to analyze a few days of the flooding event that occurred in the Metaponto plain (southern Italy) in the first week of December 2013. RST-FLOOD has been already applied using 1 km MODIS visible and near infrared data, with only a preliminarily feasibility analysis of the potential of the same data when

acquired at 250 m of spatial resolution [12]. In this work, we further assess the capability of this latter specific configuration of RST-FLOOD in detecting flooded areas, and also test its performance when implemented on VIIRS imagery data at 375 m of spatial resolution.

The main advantages of RST-FLOOD with respect to traditional techniques are: (i) the use of local (i.e., at the pixel scale) adaptive and dynamic thresholds; and (ii) no dependence on any kind of auxiliary/ancillary information [12]. Ancillary datasets or fixed thresholds on the signal under investigation are often used to face the main challenges, such as cloud and terrain shadows and the discrimination of flooded areas [34,35], limiting flood detection reliability. The accuracy/availability of auxiliary information can directly affect the quality of the achieved results, while fixed thresholds may suffer from sensitivity/accuracy limits because of the signal variability due to the specific site/local setting of the scene under investigation [14].

The only constraint for RST-FLOOD implementation is the availability of a satellite historical series long enough to guarantee a consistent identification of the expected values in terms of temporal mean and standard deviation. An independent work focusing on RST [36] found that such a historical series should consist of at least of 80 images to produce reliable reference fields, corresponding to at least three years of data, considering a monthly temporal window and a daily frequency of observation.

Results achieved by applying the RST-FLOOD indices on the two sensors suggest the benefit of their integration for a continuous monitoring of the ongoing phenomenon at large spatial scale. Such an integration enables a clear increase in the observational frequency, improving the flood evolution monitoring capability of each single sensor. This result is fundamental for decision makers, especially during the crisis, in order to better identify critical situations and ensure an effective implementation of relief and rescue operations. Furthermore, hydrological models would also benefit from the integration of continuous and updated information about the real-time situation, having the opportunity to check the quality of their setup as well as improving the quality of their outputs. Finally, the integration of multi-sensor datasets will generally increase the probability of clear sky acquisitions, reducing the impact of clouds, which are the main limitations of optical satellite observations, especially for this kind of application. It is worth mentioning that cumulated flooded maps of the event, allowed by high temporal resolution weather satellites, could help for a better delineation of the involved area, enabling an assessment and relative updating of the flooded risk map.

Basilicata rivers are representative of small hydrological basins, with small-size cross-sections (<100 m); therefore, the achieved results indicate that data acquired by medium-resolution optical sensors, if adequately analyzed, can also be profitable for flood detection monitoring of watersheds. In the near future, other test cases should be studied to further confirm the quality of the results achieved here by investigating a different scenario from the one considered here. For example, flood events of a smaller size (in terms of both channel width and floodplain extension) than the ones analyzed here should be investigated to better understand the sensitivity limit of the proposed approach when applied to data at 375 m of spatial resolution. Events occurring in urban areas should also be analyzed to confirm the feasibility of the methodology presented here. Furthermore, it is worth mentioning that while the proposed indices are almost "mandatory" for MODIS data, considering the spatial resolution constraints, VIIRS has other imagery bands, such as the I3 (SWIR: 1.58–1.64 μm), which will enable other combinations currently under investigation.

6. Conclusions

In this paper, RST-FLOOD has been applied to analyze the flood event that affected the Basilicata and Puglia regions in the first week of December 2013. Two different indicators, based on the difference and ratio between NIR and VIS reflectance (i.e., channel 2 and channel 1 for MODIS, I2 and I1 for VIIRS), respectively, have been used to detect flooded areas.

When implemented on MODIS data, the RST-FLOOD indices showed a behavior similar to the one observed when studying a different test case. A similar behavior between the two ALICE indices has been recognized, with the one based on the difference being more exposed to a few false positives due to suspended sediments flown into the San Giuliano lake. A better sensitivity of the VIIRS-based indices was observed. This aspect, which needs more investigation, can be preliminarily justified by

considering the different specific spectral and radiometric accuracies of the two sensors and the longer historical series of MODIS data.

The flood maps provided by both RST-FLOOD indices, aggregating the MODIS and VIIRS detections, are in good geographical agreement with the one derived using Landsat 7 ETM+ data of 5 December 2013. Such an integration allowed for the discrimination of a flood area extent up to 80 km^2, lower than that potentially detectable by using a high spatial resolution sensor like the ETM+ (about 24% greater). Despite this, the double advantage of an integrated system in effectively supporting flood risk management is clearly demonstrated. The high temporal revisiting capability offered by optical sensors aboard weather satellites allows for the improvement of the observational capability of an operational monitoring system, while the combined use of different indices improves the accuracy in flood extent mapping.

Author Contributions: Conceptualization, T.L., M.F., N.P. and V.T.; Methodology, T.L., N.P. and V.T.; Validation, M.F., T.L. and V.S.; Data Curation, E.C., M.F. and V.S., Writing—Original Draft Preparation, T.L., M.F. and E.C.; Writing—Review & Editing, N.P. and V.T.

Funding: This research received no external funding.

Conflicts of Interest: The authors declare no conflict of interest.

References

1. International Charter "Space & Major Disasters". Annual Report. 2016. Available online: https://disasterscharter.org/documents/10180/66908/16thAnnualReport (accessed on 29 June 2018).
2. Sanyal, J.; Lu, X.X. Application of Remote Sensing in Flood Management with Special Reference to Monsoon Asia: A Review. *Nat. Hazards* **2004**, *33*, 283–301.
3. Franci, F.; Mandanici, E.; Bitelli, G. Remote sensing analysis for flood risk management in urban sprawl contexts. *Geomat. Nat. Hazards Risk* **2015**, *6*, 583–599, doi:10.1080/19475705.2014.913695.
4. Ward, P.J.; de Perez, E.C.; Dottori, F.; Jongman, B.; Luo, T.; Safaie, S.; Uhlemann-Elmer, S. The need for mapping, modeling, and predicting flood hazard and risk at the global scale. In *Global Flood Hazard: Applications in Modeling, Mapping, and Forecasting*, 1st ed.; Geophysical Monograph 233; Schumann, G.J.-P., Bates, P.D., Apel, H., Aronica, G.T., Eds.; John Wiley & Sons, Inc.: Hoboken, NJ, USA; American Geophysical Union: Washington, DC, USA, 2018; ISBN 978-1-119-21786-2.
5. Dasgupta, A.; Grimaldi, S.; Ramsankaran, R.; Pauwels, V.R.N.; Walker, J.P.; Chini, M.; Hostache, R.; Matgen, P. Flood mapping using synthetic aperture radar sensors from local to global scales. In *Global Flood Hazard: Applications in Modeling, Mapping, and Forecasting*, 1st ed.; Geophysical Monograph 233; Schumann, G.J.-P., Bates, P.D., Apel, H., Aronica, G.T., Eds.; John Wiley & Sons, Inc.: Hoboken, NJ, USA; American Geophysical Union: Washington, DC, USA, 2018; ISBN 978-1-119-21786-2.
6. Franci, F. The Use of Satellite Remote Sensing for Flood Risk Management. Ph.D. Thesis, Alma Mater Studiorum Università di Bologna, Bologna, Italy, 2015, doi:10.6092/unibo/amsdottorato/7181.
7. Fayne, J.; Bolten, J.; Lakshmi, V.; Ahamed, A. Optical and physical methods for mapping flooding with satellite imagery. In *Remote Sensing of Hydrological Extremes*; Lakshmi, V., Ed.; Springer: Cham, Switzerland, 2017.
8. Markert, K.L.; Chishtie, F.; Anderson, E.R.; Saah, D.; Griffin, R.E. On the merging of optical and SAR satellite imagery for surface water mapping applications. *Results Phys.* **2018**, *9*, 275–277, doi:10.1016/j.rinp.2018.02.054.
9. Sun, D.; Li, S.; Zheng, W.; Croitoru, A.; Stefanidis, A.; Goldberg, M. Mapping floods due to Hurricane Sandy using NPP VIIRS and ATMS data and geotagged Flickr imagery. *Int. J. Digit. Earth* **2016**, *9*, 427–441, doi:10.1080/17538947.2015.1040474.
10. Lacava, T.; Brocca, L.; Coviello, I.; Faruolo, M.; Pergola, N.; Tramutoli, V. Integration of optical and passive microwave satellite data for flooded area detection and monitoring. In *Engineering Geology for Society and Territory*; Springer: New York, NY, USA, 2014; Volume 3, pp. 631–635.
11. Brakenridge, G.R. Flood risk mapping from orbital remote sensing. In *Global Flood Hazard: Applications in Modeling, Mapping, and Forecasting*, 1st ed.; Geophysical Monograph 233; Schumann, G.J.-P., Bates, P.D., Apel, H., Aronica, G.T., Eds.; John Wiley & Sons, Inc.: Hoboken, NJ, USA; American Geophysical Union: Washington, DC, USA, 2018; ISBN 978-1-119-21786-2.

12. Faruolo, M.; Coviello, I.; Lacava, T.; Pergola, N.; Tramutoli, V. A multi-sensor exportable approach for automatic flooded areas detection and monitoring by a composite satellite constellation. *IEEE Trans. Geosci. Remote Sens.* **2013**, *51*, 2136–2149, doi:doi:10.1109/TGRS.2012.2236336.
13. Tramutoli, V. Robust Satellite Techniques (RST) for Natural and Environmental Hazards Monitoring and Mitigation: Theory and Applications. In Proceedings of the Fourth International Workshop on the Analysis of Multitemporal Remote Sensing Images, Louven, Belgium, 18–20 July 2007.
14. Lacava, T.; Filizzola, C.; Pergola, N.; Sannazzaro, F.; Tramutoli, V. Improving flood monitoring by the Robust AVHRR Technique (RAT) approach: The case of the April 2000 Hungary flood. *Int. J. Remote Sens.* **2010**, *31*, 2043–2062.
15. Sheng, Y.; Su, Y.; Xiao, Q. Challenging the cloud-contamination problem in flood monitoring with NOAA/AVHRR imagery. *Photogramm. Eng. Remote Sens.* **1998**, *64*, 191–198.
16. Sheng, Y.; Gong, P.; Xiao, Q. Quantitative dynamic flood monitoring with NOAA AVHRR. *Int. J. Remote Sens.* **2001**, *22*, 1709–1724.
17. Xiao, Q.; Chen, W. Songhua River flood monitoring with meteorological satellite imagery. *Remote Sens. Inf.* **1987**, *4*, 37–41.
18. Centro Funzionale Decentrato delle Protezione Civile Basilicata: Eventi Metereologici Eccezionali dei Giorni 1,2 e 3 Dicembre 2013 nel Territorio della Regione Basilicata. 2013. Available online: http://www.centrofunzionalebasilicata.it/ew/ew_pdf/r/Report%20evento%20dicembre%202013.pdf (accessed on 29 June 2018).
19. Autorità di Bacino della Puglia: Valutazione Globale Provvisoria del Piano di Gestione del Rischio di Alluvioni. 2015. Available online: http://www.adb.puglia.it/public/files/downloads/20151104_PGRA/VGP.pdf (accessed on 29 June 2018).
20. Dal Sasso, S.F.; Cantisani, A.; Lanorte, V.; Pacifico, G.; Manfreda, S. Gli eventi storici della Basilicata. In *Le Precipitazioni Estreme in Basilicata*, 1st ed.; Manfreda, S., Sole, A., De Costanzo, G., Eds.; Universosud Società Cooperativa: Potenza, Italy, 2015; pp. 6–24, ISBN 978-88-99432-03-4. Available online: http://www.centrofunzionalebasilicata.it/it/pdf/pioggia_download.pdf (accessed on 29 June 2018).
21. D'addabbo, A.; Refice, A.; Pasquariello, G.; Lovergine, F.P.; Capolongo, D.; Manfreda, S. A Bayesian network for flood detection combining SAR imagery and ancillary data. *IEEE Trans. Geosci. Remote Sens.* **2016**, *54*, 3612–3625, doi:10.1109/TGRS. 2016.2520487.
22. De Musso, N.M.; Capolongo, D.; Refice, A.; Lovergine, F.P.; D'Addabbo, A.; Pennetta, L. Spatial evolution of the December 2013 Metaponto plain (Basilicata, Italy) flood event using multi-source and high-resolution remotely sensed data. *J. Maps* **2018**, *14*, 219–229, doi:10.1080/17445647.2018.1454349.
23. Il Giornale della Protezione Civile: Rassegna Stampa del 4/12/2013. 2013. Available online: https://www.ilgiornaledellaprotezionecivile.it/html/download.html?id=7315738794M (accessed on 29 June 2018).
24. Di Polito, C.; Ciancia, E.; Coviello, I.; Doxaran, D.; Lacava, T.; Pergola, N.; Satriano, V.; Tramutoli, V. On the Potential of Robust Satellite Techniques Approach for SPM Monitoring in Coastal Waters: Implementation and Application over the Basilicata Ionian Coastal Waters Using MODIS-Aqua. *Remote Sens.* **2016**, *8*, 922, doi:10.3390/rs8110922.
25. Autorità di Bacino della Basilicata: Mappe della Pericolosità e Mappe del Rischio Idraulico, Relazione. 2014. Available online: http://www.adb.basilicata.it/adb/Pstralcio/pianoacque/Relazione_ottobre_2014.pdf (accessed on 29 June 2018).
26. Level-1 and Atmosphere Archive & Distribution System (LAADS) Distributed Active Archive Center (DAAC) Archive. 2018. Available online: https://ladsweb.modaps.eosdis.nasa.gov/ (accessed on 29 June 2018).
27. NOAA Comprehensive Large Array-Data Stewardship System (CLASS). 2018. Available online: https://www.avl.class.noaa.gov/saa/products/welcome (accessed on 29 June 2018).
28. U.S. Geological Survey (USGS). EarthExplorer. 2018. Available online: https://earthexplorer.usgs.gov/ (accessed on 29 June 2018).
29. Szabó, S.; Gácsi, Z.; Balázs, B. Specific features of NDVI, NDWI and MNDWI as reflected in land cover categories. *Landsc. Environ.* **2016**, *10*, 194–202, doi:10.21120/LE/10/3-4/13.
30. Cuomo, V.; Filizzola, C.; Pergola, N.; Pietrapertosa, C.; Tramutoli, V. A self-sufficient approach for GERB cloudy radiance detection. *Atmos. Res.* **2004**, *72*, 39–56, doi:10.1016/j.atmosres.2004.03.030.

31. Pietrapertosa, C.; Pergola, N.; Lanorte, V.; Tramutoli, V. Self Adaptive Algorithms for Change Detection: OCA (the One-channel Cloud-detection Approach) an adjustable method for cloudy and clear radiances detection. In Proceedings of the Technical Proceedings of the Eleventh International (A)TOVS Study Conference (ITSC-XI), Budapest, Hungary, 20–26 September 2000; pp. 281–291.
32. Vivi Castelleneta: Alluvione a Castellaneta Marina, Case in Pericolo. 2013. Available online: http://www.vivicastellaneta.it/notizie/item/2140-alluvione-a-castellaneta-marina-case-in-pericolo (accessed on 29 June 2018).
33. Lacava, T.; Ciancia, E.; Coviello, I.; Di Polito, C.; Faruolo, M.; Pergola, N.; Satriano, V.; Tramutoli, V. A satellite multi-sensor approach for flooded areas detection and monitoring. In *Advances in Watershed Hydrology*; Moramarco, T., Barbetta, S., Brocca, L., Eds.; Water Resources Publications, LLC.: Highlands Ranch, CO, USA, 2015; Chapter 5, pp. 83–96, ISBN:13-978-1-887201-85-8.
34. Huang, C.; Chen, Y.; Wu, J.; Li, L.; Liu, R. An evaluation of Suomi NPP-VIIRS data for surface water detection. *Remote Sens. Lett.* **2015**, *6*, 155–164, doi:10.1080/2150704X.2015.1017664.
35. Li, S.; Sun, D.; Goldberg, M.D.; Sjoberg, B.; Santek, D.; Hoffman, J.P.; DeWeese, M.; Restrepo, P. Lindsey, S., Holloway, E., Automatic near real-time flood detection using Suomi-NPP/VIIRS data. *Remote Sens. Environ.* **2018**, *204*, 672–689, doi:10.1016/j.rse.2017.09.032.
36. Koeppen, W.C.; Pilger, E.; Wright, R. Time series analysis of infrared satellite data for detecting thermal anomalies: A hybrid approach. *Bull. Volcanol*. **2011**, *73*, 577–593, doi:10.1007/s00445-010-0427-y.